Rate Coefficients for the Propargyl Radical Self-Reaction and Oxygen Addition Reaction Measured Using Ultraviolet Cavity Ring-down Spectroscopy

ARTICLE *in* THE JOURNAL OF PHYSICAL CHEMISTRY A · MAY 1999

Impact Factor: 2.69 · DOI: 10.1021/jp990468s

2 AUTHORS, INCLUDING:

Jeffrey W Hudgens
National Institute of Standards and Technolo…
135 PUBLICATIONS **2,243** CITATIONS

Rate Coefficients for the Propargyl Radical Self-Reaction and Oxygen Addition Reaction Measured Using Ultraviolet Cavity Ring-down Spectroscopy

Dean B. Atkinson*,† and Jeffrey W. Hudgens*,‡

Physical and Chemical Properties Division Chemical Science and Technology, Laboratory National Institute of Standards and Technology Gaithersburg, Maryland 20899

Received: February 8, 1999; In Final Form: March 30, 1999

By using 193 nm laser photolysis and cavity ring-down spectroscopy to produce and monitor the propargyl radical (CH_2CCH), the self-reaction and oxygen termolecular association rate coefficients for the propargyl radical were measured at 295 K between total pressures of 300 Pa and 13300 Pa (2.25 and 100 Torr) in Ar, He, and N_2 buffer gases. The rate coefficients obtained by simple second-order fits to the decay data were observed to vary with the photolytic precursors: allene, propargyl chloride, and propargyl bromide. By using a numerical fitting routine and more comprehensive mechanisms, a distinct rate coefficient for the self-reaction was determined, $k_\infty(C_3H_3+C_3H_3) = (4.3 \pm 0.6) \times 10^{-11}$ cm^3 molecule^{-1} s^{-1} at 295 K. This rate coefficient, which is a factor of 2.8 times slower than reported previously, was independent of total pressure and buffer choice over the entire pressure range. Other rate coefficients derived during the modeling included $k(C_3H_3+H$ 665 Pa He$) = (2.5 \pm 1.1) \times 10^{-10}$ cm^3 molecule^{-1} s^{-1}, $k(C_3H_3+C_3H_3Cl_2) = (7 \pm 4) \times 10^{-11}$ cm^3 molecule^{-1} s^{-1}, and $k(C_3H_3+C_3H_3Br_2) = (2.4 \pm 2) \times 10^{-11}$ cm^3 molecule^{-1} s^{-1}. The association reaction $C_3H_3 + O_2$ was found to lie in the falloff region between linear and saturated pressure dependence for each buffer gas (Ar, He, and N_2) between 300 Pa and 13300 Pa. A fit of these data derived the high-pressure limiting rate coefficient $k_\infty(C_3H_3+O_2) = (2.3 \pm 0.5) \times 10^{-13}$ cm^3 molecule^{-1} s^{-1}. Three measurements of the propargyl radical absorption cross-section obtained $\sigma_{332.5} = (413 \pm 60) \times 10^{-20}$ cm^2 molecule^{-1} at 332.5 nm. Stated uncertainties are two standard deviations and include the uncertainty of the absorption cross section, where appropriate.

Introduction

Propargyl ($\bullet CH_2C{\equiv}CH$) is the simplest unsaturated hydrocarbon radical possessing resonance stabilization. This resonance stabilization energy, estimated at approximately 36 kJ mol^{-1},[1,2] accounts for its resistance to pyrolysis and relatively slow reaction rate with molecular oxygen. The suppression of these destruction mechanisms enables large concentrations of propargyl radicals to exist in flames. In flames the dominant loss channel for propargyl radicals becomes its self-reaction, which resonance stabilization does not diminish, and this channel produces acyclic C_6H_6 species. According to a mechanism proposed by Miller et. al.,[3] these acyclic C_6H_6 species cyclize to form benzene which feeds the production channels leading to polycyclic aromatic hydrocarbons (PAHs), the major component of soot. In a sense, the soot producing capacity of the propargyl radical resides in the enhancement of the ratio of its self-reaction rate over all other oxidation and pyrolysis loss rates.

Surprisingly, the reaction rate coefficients for the propargyl radical self-reaction and oxidation as well as reactions with other closed-shell molecules and radicals have been subjected to little study. The archival literature contains only two high temperature determinations[4,5] of the bimolecular reaction

$$C_3H_3 + C_3H_3 (+M) \rightarrow \text{products} \qquad (1)$$

and one recent room temperature (300 K) study.[6] One reason for this paucity of kinetic data is that the ultraviolet (UV) absorption bands of the propargyl radical near 330 nm are diffuse and relatively weak, making the sensitive and quantitative detection of the radical difficult.

During a recent study, Morter, et al.[6] monitored C_3H_3 ($\tilde{X}^2B_1$) radicals in their ground electronic state using long path color center infrared (IR) laser absorption by the acetylenic CH stretching vibration. The production of the radical was via the same photolysis sequences used in the current study. The previous study reports a rate coefficient at 295 K, $k_1 = 1.2 \pm 0.2 \times 10^{-10}$ cm^3 molecule^{-1} s^{-1}, which is derived by fitting to a simple second-order decay (i.e., disregarding other possible reactive loss channels which can contribute to propargyl radical destruction.) This rate coefficient is around 5 times larger than those found for the self-reactions of analogous saturated and resonance stabilized, unsaturated hydrocarbon radicals (e.g., *n*-propyl $k_\infty = 1.7 \times 10^{-11}$ cm^3 molecule^{-1} s^{-1}, allyl $k_\infty = 2.65 \times 10^{-11}$ cm^3 molecule^{-1} s^{-1}),[7,8] suggesting that a remeasurement of k_1 is warranted. Here, we report an experimental determination of k_1 at 295 K that is a factor of 2.8 times slower than that reported previously by Morter et al.[6]

Slagle and Gutman[9] used the sampled reactor/mass spectrometric method to study the complex behavior of the molecular oxygen addition reaction,

$$C_3H_3 + O_2 (+M) \rightarrow \text{products} \qquad (2)$$

over a wide temperature range (293−900 K). This reaction was studied at low nitrogen pressures (<300 Pa) and appeared to be in the falloff region between the high and low-pressure limits;

† NIST/NRC Postdoctoral Associate 1995−97. Current address: Chemistry Department, Portland State University, Portland, OR 97207-0751. E-mail: atkinsond@pdx.edu.

‡ E-mail: jeffrey.hudgens@nist.gov.

10.1021/jp990468s
Published on Web 05/12/1999

however, instrumental limitations did not allow a detailed investigation of the pressure dependence. At lower temperatures (293−333 K) Slagle and Gutman inferred that reaction 2 initially forms an adduct, propargylperoxy radical, but they could not rule out activity along other product channels. As temperature increases, the reaction appears to shift from pure addition (producing propargylperoxy radical), through an intermediate region (380−430 K) where equilibrium is established between the free $C_3H_3 + O_2$ and the propargylperoxy radical (which samples a barrier to products including ketene), and to higher temperatures (500−900 K) where the dominant products are ketene and formyl radicals.[9] At all temperatures the initial step in the mechanism is the addition of oxygen to propargyl, and this rate is slow relative to addition rates observed for analogous nonresonance stabilized hydrocarbon radicals.

In this work we describe measurements of the rate coefficients for reactions 1 and 2 at room temperature (295 K) and pressures between 300 Pa and 13300 Pa (2.25 and 100 Torr) of He, Ar, and N_2. Propargyl concentrations were monitored using a recently developed laser photolysis/cavity ring-down apparatus.[10] Previously reported[11] and confirmed[12] UV absorption bands were used to monitor the propargyl radical concentration during the kinetic measurements. These studies used kinetic data produced by three different photolytic precursors of propargyl radical. By modeling the complex chemical environment associated with the photolysis products of each precursor, a single, self-reaction rate coefficient for propargyl radicals is obtained. We also report analyses of the stable photolysis products of propyne and propargyl chloride.

Experimental Procedure[13]

The details of the laser photolysis/cavity ring-down (CRD) apparatus are comprehensively described elsewhere,[10] so this section presents only a basic overview and recent experimental refinements. A 16 mm i.d. quartz tube forms the reactor through which a premixed gas of known composition flows. The pumping rate is adjusted so that the movement of the gas sample along the flow axis is inconsequential within the time interval of a single kinetic measurement, yet fast enough that the reaction mixture is fully refreshed during the 200 ms between photolysis laser pulses.

Initially, an excimer laser (ArF−193 nm, nominal 20 ns pulse, maximum pulse energy 100 mJ, or XeF−351 nm, nominal 20 ns pulse, maximum pulse energy 200 mJ) photolyzes the reaction mixture. The photolysis laser beam is expanded and masked to produce a uniform block 67 mm wide and 20 mm high with a peak power density of less than 100 kW/cm^2. Subsequently, the absorption by propargyl radicals is measured using cavity ring-down spectroscopy. For the CRDS we use a 1.08 m long cavity formed by two 1.0 m radius of curvature mirrors (VLOC, Inc.) of high peak effective reflectivity ($R^* >$ 99.8% at 340 nm) and a usable bandwidth of greater than ±30 nm ($R^* >$ 98%), giving a typical base ring-down time of ≈1.3 μs. The ring-down cavity lies along the flow axis, normal to the photolysis beam direction, so that the width of the photolysis beam defines the path length for the absorbance measurement. This optical configuration makes the extraction of species density straightforward. To minimize effects from radial gradients of photolysis products, the photolysis beam height is larger than the diameter of the reactor tube and the probe beam diameter inside the cavity (beam waist of $TEM_{max} \approx 0.32$ mm) is much smaller than the flow tube inner dimension.

The tunable probe laser beam was produced by an excimer pumped dye laser (nominal 20 ns pulse width; laser dyes: DCM (610−680 nm), PTP (335−350 nm), and DMQ (345−360 nm), as well as the KDP* doubling crystal (305−340 nm)). At the cavity entrance mirror, an iris apertured the probe laser beam to ≈2 mm diameter and the energy was not allowed to exceed 100 μJ/(cm^2 pulse). The photomultiplier signal was (analog) filtered to pass frequencies less than 25 MHz. (Proper cavity alignment was verified by observing oscilloscope traces recorded at the full 1.0 GHz bandwidth.) A weighted fit to each exponential ring-down trace was extracted from a linear regression of a semilog plot and yielded the decay rate. We verified the quality of this procedure by fitting the data using an iterative, nonlinear Levenberg−Marquardt fitting routine.[14] Both methods yielded identical results. We note that CRD absorbance measurements have been demonstrated to obey the Beer−Lambert relationship for the broad transitions often encountered in the UV.[10]

Cavity ring-down measurements observe the decay rate (β) of photon intensity in a stable optical cavity. Optical absorbance is computed from the difference between the decay rates β_{abs}, the decay rate in the presence of an absorber, and β_{base}, the base decay rate under nonabsorbing conditions. The base decay rate is measured by probing the reaction mixture prior to the photolysis laser pulse. The kinetic profile of absorbing species is obtained by measuring β_{abs} over many selected delay times after the photolysis laser pulse. To compensate for the effects of system drift, we measure the average β_{base} immediately before each measurement of β_{abs}. In addition, the delay time intervals between the photolysis and CRD probe pulses are randomly selected between zero and preset values. During this study, random time sampling was particularly important because the reaction tube gradually accumulated brown soot in the photolysis region. When required, this soot was easily washed away with soap and water.

The propargyl radicals for the spectroscopic and kinetic studies were produced by 193 nm photolysis of allene, propyne, propargyl chloride, and propargyl bromide. Allene and propyne (Matheson Gas Products, stated purity 97%) were used as supplied. C_3H_3Cl (Aldrich, 98%) and C_3H_3Br (Fluka, 98%) were freeze−thaw degassed in liquid nitrogen to remove any volatile contaminants and then 5% to 10% mixtures in the buffer gas were prepared and stored in blackened glass bulbs. All reactant and buffer gases were flowed through mass flow controllers (MKS Model 1259C). To eliminate concerns about the possible destruction of alkyne halides on the metal surfaces within the flow controllers, we repeated some experiments by flowing mixtures through an all-Teflon needle valve. These experiments yielded results identical to those that used flow controllers.

During measurements of the nearly pseudo-first-order rate coefficients for reaction 2, it was necessary to establish the absolute density of the oxygen. The concern was that mixing between the continuously flowing reactor and backflush zones might perturb the O_2 density. (The backflush is used to minimize mirror contamination.) In the flow reactor the O_2 fractional flow rate is multiplied by the total pressure to obtain the partial pressure, which is then converted to a density. During this calculation we implicitly assume that all of the O_2 flow is entrained within the flow of the central section of the reactor, i.e., the central flow and the backflush flow do not mix. Significant mixing could lead to negative determinate errors in the O_2 density and adversely affect the derived rate coefficients for reaction 2. During a recent study[10] we investigated this potential problem by measuring the rate coefficient for $C_2H_5 + O_2$ and by measuring the absorption cross-section of Cl_2. Both measurements are sensitive to mixing between the backflush

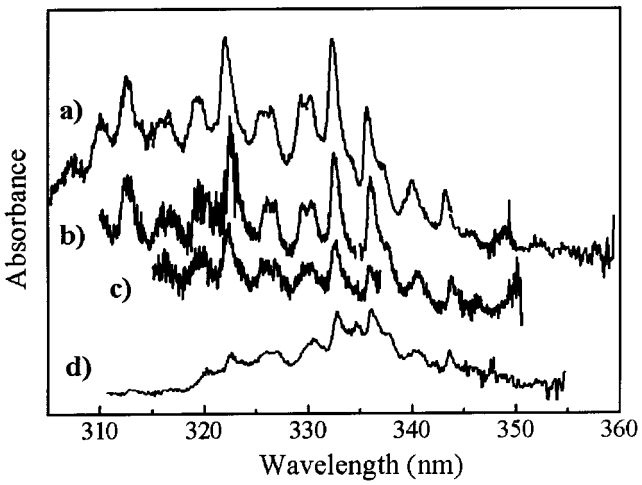

Figure 1. Ultraviolet absorption spectra of the propargyl radical, C_3H_3, observed from the 193 nm photolysis of (a) propyne, (b) allene, (c) propargyl chloride, and (d) propargyl bromide. The vertical scale factor of each plot is arbitrary and selected for presentation clarity.

and the central reactor flows. Using procedures and reactor conditions similar to those reported here, this apparatus obtained close agreement with accepted literature values. Therefore, we conclude that effects induced by mixing are insignificant.

GC−MS end-product analyses of irradiated samples were accomplished with a HP 5890 Series 2 gas chromatograph (GC) that is coupled to a HP 5972 mass spectrometer. The GC was equipped with a Restek Model 502.2 column (0.32 mm i.d. × 30 m long). A bulb equipped with fused quartz windows was filled with a 1% C_3H_3Cl/99% He mixture to 101 kPa (1 atm) and irradiated with 100 ArF laser pulses at 30 mJ/pulse at 1 Hz. In other experiments, the bulb was filled with 6.5% propyne/93.5% Ar mixture to 101 kPa and irradiated with 500 ArF laser shots at 30 mJ/pulse at 1 Hz. These exposures were the smallest needed to generate measurable quantities of photolysis products from each precursor. The irradiated samples were injected into a gas chromatograph and the mass spectra of the eluted peaks were recorded.

The kinetic experiments produce transient absorption (which is readily converted to radical concentration) vs time. To derive rate coefficients from these data, the kinetic mechanism is designed and the absorption data is computationally simulated on a computer. This simulation is compared to the observed data and the χ^2 value is computed. Using the Levenberg−Marquardt procedure,[14] selected rate coefficients and concentrations are varied to minimize this value. The simulation software is comprised of a customized graphic interface that spawns satellite shells executing the original FORTRAN code of the ACUCHEM kinetics simulation program.[15] ACUCHEM contains a symbolic interpreter, allowing the input of the kinetic model in an intuitive format, and a numerical forward integration routine, the accuracy of which has been described and verified previously.[15]

Results

Propargyl Radical Spectrum between 310 and 360 nm. Figure 1 shows absorption spectra of the flow reactor contents observed 10 μs after propyne, allene, propargyl chloride, and propargyl bromide are photolyzed by 193 nm laser light. Although the spectra between 305 and 360 nm exhibit varied band shapes and relative intensities, their band maxima align indicating that they originate from the same spectral carrier. As the time interval between the photolysis and probe pulses was increased to ≈10 ms, the spectral bands decayed and finally vanished, thus establishing the transient nature of the spectral carrier.

TABLE 1: Spectral Features Observed in UV Absorption Spectra of the Propargyl Radical (C_3H_3 ($\tilde{X}^2B_1$)) during This Work and Previous Studies

gas-phase CRDS (peak,[a] nm)	gas-phase UV absorption (bandhead,[b] nm)	Ar-matrix UV absorption (peak,[c] nm)
352.8 (weak)		
349.3		
346.3		346.8
343.6	343.2	342.8
340.3	340.3	339.1
335.9	335.6	335.2
332.5	332.0	332.4
329.5/330.4 (doublet)	329.2	328.5
325.6/326.6 (doublet)	325.2	324.8
322.1	321.7	321.7
319.4	318.9	318.5
315.7/316.5 (doublet)	315.4	315.0
312.5	311.9	
309.9	309.5	
307.4	305.6	305.8
	303.0	303.0
	300.3	

[a] This work. Absolute uncertainty of band centers is ≤ ±0.50 nm. [b] From ref 11. Stated uncertainty for each bandhead ranges between ±0.5 and ±1.0 nm. [c] From ref 12.

Table 1 lists the UV absorption maxima observed in the present gas-phase CRD spectrum, the UV absorption bandheads reported from the gas-phase study by Ramsey and Thistlethwaite,[11] and the absorption maxima observed during the argon cryogenic matrix study by Jacox and Milligan.[12] The agreements among the band positions show that the present and prior studies have examined the same transient species. Ramsey and Thistlethwaite[11] established that this UV spectrum originates from the propargyl radical. Jacox and Milligan[12] showed that the growth and destruction of these UV bands by species entrained in a cryogenic argon matrix were mirrored by a set of infrared absorption bands. Although this electronic band system has not been assigned, this correlation establishes that the UV absorption bands arise from the vibrationless energy level of the ground electronic state. The accord between the infrared data and the results of ab initio calculations[16,17] confirms further that the propargyl radial carried the IR spectrum, and by inference, that propargyl radical carries the UV spectrum. Ab initio calculations also predict that an ultraviolet band system of the propargyl radical resides in the 330 nm region.[16,18] Thus, we assign the CRD spectrum to arise from the vibrationless propargyl radical in its ground electronic state, i.e., C_3H_3 ($\tilde{X}^2B_1$).

In Figure 1 the spectra obtained from the four different precursors show slight variations in peak shape and relative intensity, particularly for the propargyl bromide precursor. Most of these variations seemed to originate from the substantial degradation of the photolysis energy during each scan. This degradation was caused by soot accumulation on the reactor tube walls (through which the photolysis beam passes). This sooting does not affect the CRDS absorption measurement, which is made by a comparison of the ring-down rates before and after the photolysis pulse, nor does it necessarily degrade the cavity mirror performance. Sooting does, however, affect the amount of propargyl radicals produced per photolysis pulse. As soot accumulates, the amount of transient species (C_3H_3) decreases but the background noise remains constant. Thus, the signal-to-noise ratio (S/N) also decreases and smaller features "wash out", e.g., the doublet splitting of the 326 nm peaks.

In an attempt to correct for these phenomena, the spectra produced from propargyl bromide and propyne were recorded in small segments and the photolysis power transmitted through the reactor was monitored. When the photolysis energy transmitted into the flow tube decreased to 50%, we terminated data collection and a linear correction was applied to the scan segment. This power correction procedure is legitimate because we also verified that the absorption signal is a linear function of the photolysis power. However, this procedure cannot compensate for the deterioration of the *S*/*N* ratio. For example, the photolysis products of propargyl bromide (Figure 1d) that generate the greatest amount of soot also exhibit a spectrum that suffers the greatest variation in relative intensity and band shapes. Conversely, the photolysis products of propyne and allene that generate less soot exhibit spectra with better reproducibility. Presumably, the reaction of nascent H-atoms with C_3H_3 radicals (see below) suppresses the soot production mechanism when propyne and allene are photolyzed. We note that the spectral distortions from soot arise during the $\approx 10^5$ laser shots used to produce each spectrum. In contrast, each kinetic measurement is obtained with only $\approx 10^3$ laser shots. During each kinetic measurement the average photolysis energy diminished by less than 1%.

For the kinetic studies, we also wish to establish that propargyl radicals account for all absorbance at 332.5 nm. Current knowledge is sufficient to dismiss the possibility of interference by other species. Each precursor photodissociates along two channels:

$$C_3H_3X + 193\ \text{nm} \rightarrow C_3H_3 + X\ (X = H, Cl, Br) \quad (3a)$$

$$\rightarrow C_3H_2 + HX \quad (3b)$$

Previous studies have reported the 193 nm C_3H_3 photolysis yields from allene (89%[19] and 64%[20]) propyne (56%[20]), propargyl chloride (93%),[6] and propargyl bromide (<50%).[21] Allene and propyne photodissociate to form vinylidene carbene ($CH_2C{=}C{:}$).[19,20,22−24] The C_3H_2 product of the propargyl halides is not established, but the candidates are the propadienylidene ($CH_2{=}C{=}C{:}$), propynylidene ($H\dot{C}{=}C{=}\dot{C}H$), and cyclopropenylidene structures. The absorption bands of these species do not overlap the propargyl band system.[25,26] An electronically excited singlet state of propynylidene is reported to exhibit diffuse bands between 310 and 370 nm,[27] but the CRD spectrum does not exhibit features indicating its presence. Any absorbance by singlet propynylidene is very small (<1% of the propargyl radical absorbance) or absent.

To account for all possible reactions that may follow reaction 3, complex kinetic schemes can be devised that generate a wide variety of major and minor transient products. Among these are the allyl, C_3, C_2H, $C_3H_3Cl_2$, and $C_3H_3Br_2$ radicals. The spectra of these species are well-characterized and do not absorb at 332.5 nm.[28−30] Thus, we conclude that all absorbance at 332.5 nm arises from the propargyl radical.

During our experiments we tried generating propargyl radicals by reacting chlorine atoms with propyne and allene. These experiments produced no detectable transient absorption in the region around 330 nm. The absence of detectable absorption implies that hydrogen abstraction from these precursors is inefficient at 295 K and that these reactions are not useful propargyl radical sources.

Transient Absorption Signals between 215 and 280 nm. An examination of the other spectral regions accessible to our CRD mirrors (215−225 nm, 238−250 nm, and 262−280 nm) found absorbance by other transient species. These transient absorbance signatures were distinct from the propargyl radial. We report the characterization and kinetic measurements of these species in a separate account.[30] Photolysis of the propargyl halides at 193 nm produced strong transient absorption around 238 nm. The kinetic behavior suggested that the spectral carriers were the chlorine and bromine adducts of the parent compounds formed by the reaction,

$$C_3H_3X + X\ (+ M) \rightarrow C_3H_3X_2 \quad (4)$$

We confirmed this assignment by observing the same absorption spectrum and similar kinetic behavior from mixtures of chlorine and propargyl chloride that were exposed to 351 nm laser light. Under these conditions Cl_2 dissociates, propargyl chloride remains photolytically inert, and reaction 4 is the only channel that can account for the increased transient absorption.

The 193 nm photolysis products of propargyl bromide exhibited a prompt increase in absorbance between 240 and 250 nm, indicating that the absorption originates from one of both nascent photolysis products, C_3H_3 or C_3H_2. Because photolysis of propargyl chloride, which has a much larger quantum yield for C_3H_3 (≈90%) than that for C_3H_3Br (≈50%), did not produce strong prompt absorption, we can rule out C_3H_3 and assign the absorption to one of the C_3H_2 carbenes. Because it absorbs strongly between 240 and 250 nm,[25,26] vinylidene carbene ($CH_2C{=}C{:}$) is the most likely carrier of this signal. Assignments to the propynylidene or cyclopropenylidene structures are not supported because they do not absorb over this spectral interval.[25]

Analyses of the Stable Photolysis Products. Three studies have reported that photolysis of propyne by 193 nm light proceeds via loss of the acetylenic hydrogen, e.g.,

$$CH_3C{\equiv}CH + 193\ \text{nm} \rightarrow CH_3C{\equiv}C\bullet + H \quad (5)$$

rather than hydrogen loss at the methyl group.[20,31,32] The appearance of the propargyl radical spectrum following the 193 nm photolysis event seems at odds with these results. To test the dominance of reaction 5 and persistence of any 1-propynyl radical ($CH_3C{\equiv}C\bullet$) product, we conducted a series of experiments that analyzed the gaseous photolysis products present after propargyl radical precursors were exposed to 193 nm light.

The GC−MS analysis of the major gaseous photolysis products of propargyl chloride found two distinct C_6H_6 species, two $C_3H_4Cl_2$ species, and two C_3H_3Cl species (chloro-allene and the parent propargyl chloride.) The GC−MS reference data confirmed that the dominant C_6H_6 species is 1,5-hexadiyne. This product is consistent with the self-reaction of propargyl radical where addition occurs at the methylenic sites, e.g.,

$$HC{\equiv}CCH_2\bullet + \bullet CH_2C{\equiv}CH\ (+M) \rightarrow HC{\equiv}C{-}CH_2{-}CH_2C{\equiv}CH \quad (6)$$

The mass spectrum of the second C_6H_6 species[33] is consistent with the structure of 1,2-hexadien-5-yne; however, no reference spectrum for this compound is available to confirm the assignment. The self-reaction of propargyl radical has been shown[4] to produce 1,2-hexadien-5-yne via a condensation reaction at the acetylenic and methylenic carbons, e.g.,

$$CH_2{=}C{=}CH\bullet + \bullet CH_2C{\equiv}CH\ (+M) \rightarrow H_2C{=}C{=}CH{-}CH_2C{\equiv}CH \quad (7)$$

The GC−MS analysis of the photolysis products of propyne found the same two C_6H_6 species as observed in the propargyl

chloride sample; two distinct, but minor, C_6H_8 species and one minor C_4 species. The total ion current (TIC) of the minor species was less than 5% of the TIC from the C_6H_6 species. Both C_6H_6 photolysis products were compared with reference GC−MS analyses obtained from a commercial sample of 2,4-hexadiyne. Neither C_6H_6 photolysis product matched the reference data for 2,4-hexadiyne. The self-reaction of $CH_3C{\equiv}C\bullet$ is expected to produce 2,4-hexadiyne via:

$$CH_3C{\equiv}C\bullet + \bullet C{\equiv}CCH_3\ (+M) \rightarrow CH_3C{\equiv}C{-}C{\equiv}CCH_3 \quad (8)$$

therefore, the absence of 2,4-hexadiyne from the C_6H_6 photolysis products indicates that little or no $CH_3C{\equiv}C\bullet$ is available (or has persisted long enough) to undergo self-reactions.

We identified the $C_3H_4Cl_2$ eluents by matching their retention times and mass spectra with standards. The dominant (>95%) $C_3H_4Cl_2$ product is 2,3-dichloro-1-propene and a second, almost undetectable (<5%) eluent proved to be *cis*-1,3-dichloro-1-propene. Our GC−MS apparatus did not detect any *trans*-1,3-dichloro-1-propene, even though it cleanly resolves the three $C_3H_4Cl_2$ isomers. The GC−MS data suggest that reaction 4 produces mainly the 2,3-dichloro-1-propene-1-yl radical and a small amount of the 1,3-dichloro-1-propene-2-yl radical. The 2,3-dichloro-1-propene-1-yl radical is the spectral carrier at 242 nm in our parallel kinetic studies of the chlorine adducts of propargyl chloride. In summary, the absorption spectra (Figure 1) and end-product data indicate that 193 nm photolysis of propyne and propargyl chloride generates significant amounts of propargyl radicals. If propyne photolysis proceeds via reaction 5, nascent $CH_3C{\equiv}C\bullet$ photoproducts must be rapidly converted to propargyl radicals in our high-pressure reactor. We also note that the presence of $C_3H_4Cl_2$ species among the end-products of the propargyl chloride sample is consistent with the activity of reaction 4 following photolysis.

Measurements of the Absorption Cross Section of C_3H_3. The largest peak in the UV spectrum (Figure 1), centered on 332.5 nm, was used to measure propargyl radical concentrations. Within the bandwidth of our laser ($\Delta\nu \approx 0.3$ cm^{-1}) the spectrum of this band exhibits no fine structure. Indeed, Ramsey and Thistlethwaite[11] used a 6.7 m spectrometer to collect much higher resolution spectra and established that these bands are "truly diffuse". They attributed the homogeneous broadening of these bands to predissociation. Diffuse continuum spectra are ideal for absorption measurements with cavity ring-down spectroscopy. The extinction coefficient remains essentially constant across the bandwidth of the laser beam causing each populated cavity mode to decay at the same rate.[34] Thus, the 332.5 nm band should provide accurate CRD measurements of propargyl concentration.

To establish the absolute absorption cross section of the propargyl radical at 332.5 nm, we used three different calibration schemes. First, the absorption by propargyl radical at 332.5 nm was compared to the absorption by ethylperoxy radical at 270 nm. The ethylperoxy radical was formed by the reaction sequence:

$$C_3H_3Cl + 193\ \text{nm} \rightarrow C_3H_3 + Cl \quad (3a)$$

$$Cl + C_2H_6 \rightarrow HCl + C_2H_5 \quad (9)$$

$$C_2H_5 + O_2\ (+M) \rightarrow C_2H_5O_2 \quad (10)$$

Sufficient ethane and oxygen were added to ensure that >98% of the chlorine atoms produced in reaction 3a were converted to ethylperoxy radicals;[10,35] thus, the absorption measurements assayed equal amounts of propargyl and ethylperoxy radicals. The ratio of absorbances $A^{C_3H_3}_{332.5}/A^{C_2H_5O_2}_{270.0} = 2.08$ was multiplied by the recommended absorption cross section for ethylperoxy radical at 270 nm, $\sigma_{270} = 214 \times 10^{-20}$ molecule^{-1} cm^2,[35] to yield a value of 446×10^{-20} molecule^{-1} cm^2 for the propargyl radical absorption cross section at 332.5 nm.

The second scheme measured absorbance of propargyl radical at 332.5 nm and the absorbance of the primary chlorine addition product with propargyl chloride at 240 nm. Photolysis of propargyl chloride (at 193 nm) produces equal quantities of the propargyl and chlorine atoms (reaction 3a). The chlorine atoms add to the propargyl chloride parent via reaction 4, producing the adduct $C_3H_3Cl_2$ which absorbs strongly at 240.0 nm. The results of these experiments implied the ratio $A^{C_3H_3}_{332.5}/A^{C_3H_3Cl_2}_{240.0} = 0.0929$. This ratio multiplied by the absorption cross section of the $C_3H_3Cl_2$ radical at 240.0 nm, $\sigma_{240.0} = 4.16 \times 10^{-17}$ molecule^{-1} cm^2,[30] gives an absorption cross section for the propargyl radical at 332.5 nm of 386×10^{-20} molecule^{-1} cm^2.

Finally, the absorption cross section for propargyl at 332.5 nm was calculated directly from change in absorbance observed when propargyl chloride samples were photolyzed by 193 nm laser light in the flow tube. The photolysis of propargyl chloride proceeds through two channels (reaction 3) and Morter et al.[6] have measured the branching ratio for production of propargyl radical $f_{3a} = 0.93$. Fahr et al.[18] have measured the absorption cross section for propargyl chloride, $\sigma_{193} = 378 \times 10^{-20}$ molecule^{-1} cm^2. During these experiments we measured a 193 nm photolysis laser flux of 1.6 mJ/cm^2, less the 31% transmission loss measured at the curved face of the quartz flow tube. This information combined with σ_{193} and f_{3a} yields a value of 408×10^{-20} molecule^{-1} cm^2 for the absorption cross section of the propargyl radical at 332.5 nm.

Since the three measurement schemes are consistent, we recommend the mean of these measurements, $\sigma_{332.5} = (413 \pm 60) \times 10^{-20}$ molecule^{-1} cm^2, where the stated uncertainty is twice the standard deviation of the three determinations.

Self-Reaction of Propargyl Radicals. The self-reaction rate of propargyl radicals (reaction 1) was studied at 295 K by observing the decay of absorbance at 332.5 nm following the 193 nm photolysis of allene, propargyl chloride and propargyl bromide in 42 separate experiments. During each kinetic experiment we measured the average photolysis energy transmitted through the flow reactor and found that it diminished by less than 1%. The average photolysis flux across the entire sample is uniform within 10%. This uniformity characteristic exists because the photolysis beam is impinging perpendicular to the CRDS cavity, the probe beam diameter inside the cavity is small (beam waist of $TEM_{max} \approx 0.32$ mm), and the gas mixture is optically thin. We also experimentally verified that each photolysis event irradiated only fresh gas-samples. When probing at $\lambda_{crds} = 240$ nm, allene shows a small, prompt absorption that does not decay. Although we could not identify the carrier (and its appearance is too prompt to attribute to soot formation), this signal was used to establish the gas flow conditions that assured that each experiment involved a fresh gas sample. At $\lambda_{crds} = 332.5$ nm this base line shift was not observed.

For the time-resolved kinetic measurements at $\lambda_{crds} = 332.5$ nm, the reaction conditions spanned three different buffer gases (N_2, He, and Ar) at total pressures between 303 and 13300 Pa (2.28−100 Torr). The partial pressure of the photolytic precursors spanned an order of magnitude. Kinetic decays were recorded until the signal declined to about 5% of its maximum.

TABLE 2: Kinetic Model and Derived Rate Coefficients that Interpret the Signal Traces Produced by 193 nm Photolysis of C_3H_3Cl at 295 K. The Experiments Monitored the C_3H_3 Concentration at 332.5 nm

reaction	rate coefficient,[b] (cm^3 $molecule^{-1}$ s^{-1})	comments
$C_3H_3Cl + 193\ nm \rightarrow C_3H_3 + Cl$	$f_{1a} = 0.93$	Branching ratio from ref 6
$\rightarrow C_3H_2 + HCl$	$f_{1b} = 0.07$	
$C_3H_3 + C_3H_3 \rightarrow C_6H_6$	$k' = (4.2 \pm 0.9) \times 10^{-11}$	Fitted value of this study
$C_3H_3Cl + Cl \rightarrow C_3H_3Cl_2$[b]	1.2×10^{-10}	Unadjusted value from ref 30
$C_3H_3 + Cl \rightarrow C_3H_3Cl$	1.5×10^{-10}	Unadjusted value. See text
$C_3H_3Cl_2 + Cl \rightarrow C_3H_3Cl_3$	1.5×10^{-10}	Unadjusted value. See text
$C_3H_3Cl_2 + C_3H_3Cl_2 \rightarrow$ products	3.4×10^{-11}	Unadjusted value from ref 30
$C_3H_3 + C_3H_3Cl_2 \rightarrow$ products	$(7 \pm 4) \times 10^{-11}$	Fitted value of this study

[a] Uncertainties denote two standard deviations. The uncertainty of k' does not include the uncertainty of the absorption cross section for C_3H_3. [b] 2,3-Dichloro-1-propene-1-yl radical. See text and ref 30.

TABLE 3: The Kinetic Model and Derived Rate Coefficients That Interpret the Signal Traces Produced by 193 nm Photolysis of C_3H_3Br at 295 K. The Experiments Monitored the C_3H_3 Concentration at 332.5 nm

reaction	rate coefficient[a] (cm^3 $molecule^{-1}$ s^{-1})	comments
$C_3H_3Br + 193\ nm \rightarrow C_3H_3 + Br$	$f_{1a} = 0.5$	Branching ratio adopted from ref 21
$\rightarrow C_3H_2 + HBr$	$f_{1a} = 0.5$	
$C_3H_3Br + Br \rightarrow C_3H_3Br_2$[b]	2×10^{-12}	Unadjusted value from ref 30
$C_3H_3 + Br \rightarrow C_3H_3Br$	$(6.5 \pm 5) \times 10^{-11}$	Fitted value of this study
$C_3H_3 + C_3H_3 \rightarrow C_6H_6$	$k' = (4.5 \pm 2) \times 10^{-11}$	Fitted value of this study
$C_3H_3 + C_3H_3Br_2 \rightarrow$ products	$(2.4 \pm 2) \times 10^{-11}$	Fitted value of this study
$C_3H_3Br_2 + Br \rightarrow$ products	8×10^{-11}	Unadjusted value from ref 30
$C_3H_3Br_2 + C_3H_3Br_2 \rightarrow$ products	1.7×10^{-11}	Unadjusted value from ref 30
$C_3H_2 + C_3H_3Br_2 \rightarrow$ products	4×10^{-11}	Unadjusted value. See text
$C_3H_2 + Br \rightarrow C_3H_3Br$	4×10^{-11}	Unadjusted value. See text
$C_3H_3 + C_3H_2 \rightarrow$ products	5×10^{-11}	Unadjusted value. See text
$C_3H_2 + C_3H_2 \rightarrow$ products	5×10^{-11}	Unadjusted value. See text
$C_3H_2 + C_3H_3Br \rightarrow$ products	5×10^{-12}	Unadjusted value. See text

[a] Uncertainties denote two standard deviations. The uncertainty of k' does not include the uncertainty of the absorption cross section for C_3H_3. [b] Tentatively assigned to 2,3-dibromo-1-propene-1-yl radical. From ref 30.

This dynamic range corresponds to measurement of approximately four half-lives of the kinetic rate coefficient. Depletion of free radicals through wall reactions and the existence of a source channel of vibrationless C_3H_3 radicals from a nascent population of vibrationally excited, but nonabsorbing, C_3H_3 radicals may be discounted. Such processes will exhibit dependencies on the total pressure and upon the partial pressure of the photolytic precursor. Since the derived rate coefficients showed no systematic dependence on pressure or third body as conditions were changed by over more than an order of magnitude, we conclude that these potential perturbations do not influence our rate determinations.

During our initial analyses of the data obtained with halogen precursors, we used simple second-order fits of the kinetic absorption data to determine the self-reaction rate coefficient, k_1. The fits of propargyl chloride photolysis data found k_1'(second order) $= (8.3 \pm 1.7) \times 10^{-11}$ cm^3 $molecule^{-1}$ s^{-1} (24 determinations) and fits of propargyl bromide data gave k_1'(second order) $= (6.6 \pm 0.8) \times 10^{-11}$ cm^3 $molecule^{-1}$ s^{-1} (12 determinations), where the stated uncertainties reflect twice the standard deviation of the individual measurements. [In this report the uncertainty in $\sigma_{332.5}$ is propagated into unprimed rate coefficients (e.g., k_1), while primed rate coefficients (e.g., k_1') do not incorporate the uncertainty of $\sigma_{332.5}$.] The 25% difference between these derived k_1'(second order) rates is statistically significant and exists because side reactions involving C_3H_3 have accelerated the observed signal decay. Because each chemical system has a unique set of side reactions involving C_3H_3, the acceleration of the derived k_1'(second order) is a function of the photolysis precursor. Thus, we discarded this simplified approach and analyzed the data by numerical chemical modeling. These chemical models account for the contributions of side reactions that accelerate the loss of C_3H_3 and distort the determinations of k_1. This procedure has yielded a unique value of k_1 that fits the data observed from the photolysis of allene, propargyl chloride, and propargyl bromide.

Tables 2 and 3 present the full kinetic mechanisms used to fit absorption by C_3H_3 radicals following 193 nm photolysis of propargyl chloride and propargyl bromide. These models account for much of the chemical environment that affects the apparent rate of the propargyl self-reaction. The photolysis event generates halogen atoms that subsequently add to parent molecules and form 2,3-dihalo-1-propene-1-yl radicals ($C_3H_3X_2$). This concentration of $C_3H_3X_2$ radicals accelerates the decay of propargyl radicals through the cross reactions $C_3H_3 + C_3H_3X_2$.

Since the concentration of $C_3H_3X_2$ radicals can be measured at 242 nm, where C_3H_3 does not absorb, we were able to measure independently the production and self-reaction rate coefficients of these $C_3H_3X_2$ radicals in a parallel study.[30] Specifically, by monitoring absorption at 242 nm in a system devoid of propagyl radicals, we determined $k(C_3H_3Cl+Cl)$ and $k(C_3H_3Cl_2+C_3H_3Cl_2)$. Similar experiments determined $k(C_3H_3Br+Br)$, $k(C_3H_3Br_2+Br)$, and $k(C_3H_3Br_2+C_3H_3Br_2)$ in a chemical system containing C_3H_3 radicals. To derive these $C_3H_3Br_2$ rate coefficients, we included trial values of $k(C_3H_3+C_3H_3)$ derived from the final fits of the allene and propargyl chloride data. These produced an intermediate set of $C_3H_3Br_2$ rate coefficients that were used to model the C_3H_3 decay data. Modeling the C_3H_3 decay data observed at 332.5 nm from C_3H_3Br precursor produced a k' for $C_3H_3+C_3H_3$ (Table 3), which was averaged with the determinations of k' found from the C_3H_3Cl and allene data (Tables 2 and 4). This weighted average of k' gave an intermediate $k(C_3H_3+C_3H_3)$ that was used to refit the $C_3H_3Br_2$ decay data (observed at 242 nm). Since the three k' differed only slightly, this recursive modeling of both C_3H_3Br photolysis data sets (observed at 332.5 nm and at 242 nm) converged to produce an invariant set of rate coefficients after one additional cycle.

TABLE 4: The Kinetic Model and Derived Rate Coefficients That Interpret the Signal Traces Produced by 193 nm Photolysis of C_3H_4 (Allene) at 295 K. The Experiments Monitored the C_3H_3 Concentration at 332.5 nm

reaction	rate coefficient[a] cm^3 molecule^{-1} s^{-1}	comments
$C_3H_4 + 193\ nm \rightarrow C_3H_3 + H$	$f_{1a} = 0.89$	Branching ratio from ref 24
$\rightarrow C_3H_2 + H_2$	$f_{1b} = 0.11$	
$C_3H_3 + C_3H_3 \rightarrow C_6H_6$	$k' = (4.4 \pm 1.4) \times 10^{-11}$	Obtained during this study
$C_3H_3 + H \rightarrow C_3H_4$	$(2.5 \pm 1.1) \times 10^{-10}$	Obtained during this study
$C_3H_4 + H \rightarrow C_3H_5$ (allyl)	6.5×10^{-13}	Unadjusted value from ref 53
$C_3H_5 + C_3H_5 \rightarrow$ products	2.7×10^{-11}	Unadjusted value from the average of refs 38 and 39
$C_3H_3 + C_3H_5 \rightarrow$ products	2.9×10^{-11}	Unadjusted value. See text
$C_3H_5 + H \rightarrow C_3H_6$	3.3×10^{-10}	Unadjusted value from ref 54
$H + H \rightarrow H_2$	8.6×10^{-16} (665 Pa)	Unadjusted value from ref 53

[a] Uncertainties denote two standard deviations. The uncertainty of k' does not include the uncertainty of the absorption cross section for C_3H_3.

Chlorine atoms add to propargyl chloride at nearly the collision rate. The formation of bromine adduct via reaction 4 occurs much more slowly. The parallel study also measured the $C_3H_3X_2$ self-reaction and $C_3H_3X_2 + C_3H_3$ cross-reactions.[30] The derived self-reaction rate coefficient for $C_3H_3Cl_2$ is more rapid than that for $C_3H_3Br_2$. The rate coefficients of the cross-reactions C_3H_3, $C_3H_3X_2$, and C_3H_2 radicals with halogen atoms ($k(C_3H_3+Cl)$ and $k(C_3H_3Cl_2+Cl)$ in Table 2 and $k(C_3H_2+Br)$ in Table 3) were estimated by adjusting the observed rate coefficient $k(C_3H_3+Br)$ (Table 3) by the reduced masses of the reactants. This estimation procedure assumes that these radical−radical recombination reactions have no potential energy barriers and proceed at their respective reduce mass weighted collision rates times the efficiency factor derived for $k(C_3H_3+Br)$.

We note that the reaction system initiated by photolysis of C_3H_3Cl produced some of the best determinations of $k(C_3H_3+C_3H_3)$. This occurred mainly because Cl atoms are not persistent and because we have independent measurements of rate coefficients involving $C_3H_3Cl_2$. Initially, reactions involving the C_3H_2 carbene product from reaction 3 were included in each model. For the propargyl chloride model these reactions were found superfluous because the maximum concentration of C_3H_2 is less than 4% of the nascent reactive species (i.e. X, C_3H_3, and C_3H_2) produced by the photolysis event (reaction 3).[6] In contrast, the model for propargyl bromide retains these reactions because ≈33% of the reactive species generated by photolysis of propargyl bromide are C_3H_2.[21] Our parallel study at 242 nm detected the prompt production of the C_3H_2 singlet carbene among these photolysis products.[30] Modeling of the temporal absorption at 242 nm indicates that the carbene population falls to <10% of its initial value within 600 μs. The lifetime of C_3H_2 is governed mainly by its reactivity with the photolytic precursor. Since our studies did not explicitly determine this rate coefficient, we have adopted rates estimated by analogy with those reported for singlet CH_2 carbene insertion into hydrocarbons.[36] The models also use estimated carbene-radical rate coefficients of similar magnitude.

When fitting complex reaction systems, it can be difficult to separate the contributions from parallel loss channels that lead to destruction of the observable, in this case, propargyl radicals. For instance, the cross reaction ($C_3H_3 + C_3H_3X_2$) and the propargyl self-reaction ($C_3H_3 + C_3H_3$) produce very similar decay signatures since the rate coefficients have the same magnitude and the concentration of $C_3H_3X_2$ tends to track with that of the propargyl radical. Fortunately, at longer reaction times the C_3H_3 and $C_3H_3X_2$ concentrations eventually diverge enough to permit distinct solutions for $k(C_3H_3+C_3H_3X_2)$ and $k(C_3H_3+C_3H_3)$, which are reported in Tables 2 and 3. Another verification of our model is found by noting that the cross-reaction rate coefficients $k(C_3H_3+C_3H_3X_2)$ obtained from 332.5 nm data (monitoring C_3H_3, Tables 2 and 3) and determined from 242 nm data (monitoring $C_3H_3X_2$)[30] are identical.

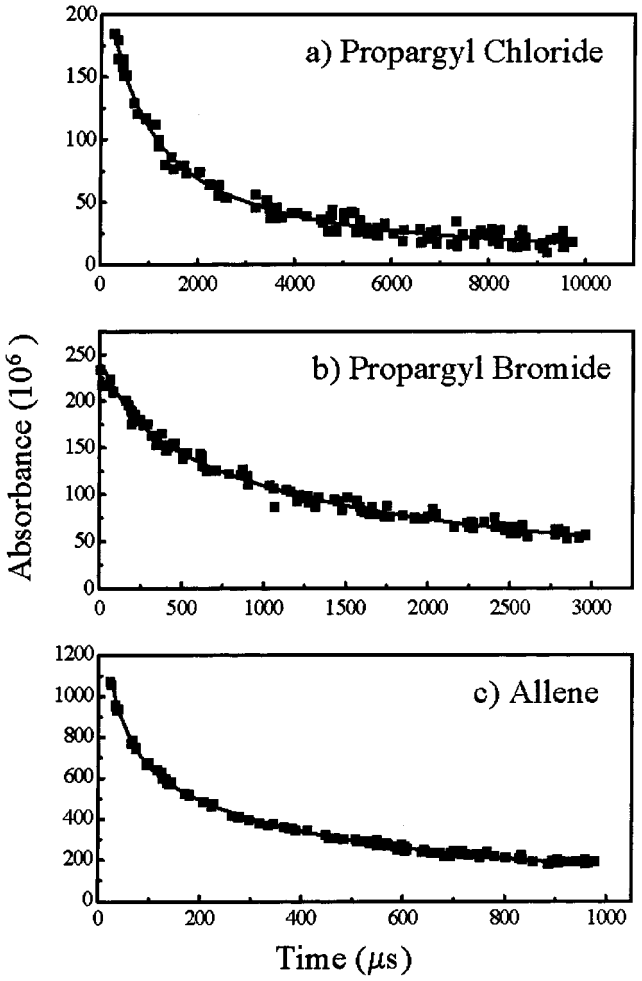

Figure 2. Plots of the transient absorbance observed at 332.5 nm following the 193 nm photolysis of propargyl radical precursors at 295 K and 600 Pa total pressure (N_2 buffer): (a) propargyl chloride; the solid line shows the fit that gives individual measurements of $k(C_3H_3 + C_3H_3)$ and $k(C_3H_3 + C_3H_3Cl_2)$. See Table 2. (b) propargyl bromide; the solid line shows the fit that gives individual measurements of $k(C_3H_3 + Br)$, $k(C_3H_3 + C_3H_3)$ and $k(C_3H_3 + C_3H_3Br_2)$. See Table 3. (c) allene; the solid line shows the fit that gives individual measurements of $k(C_3H_3+H)$ and $k(C_3H_3 + C_3H_3)$. See Table 4.

Figure 2a shows typical experimental data observed for the photolysis of propargyl chloride. The line shows the fit computed by the kinetic model (Table 2) and its good agreement with the data. Because the Cl atom concentration is depleted within the first ≈30 to ≈50 μs by addition to propargyl chloride, we could ignore side reactions between Cl and other species. Fits of the data showed no evidence for a pseudo-first-order

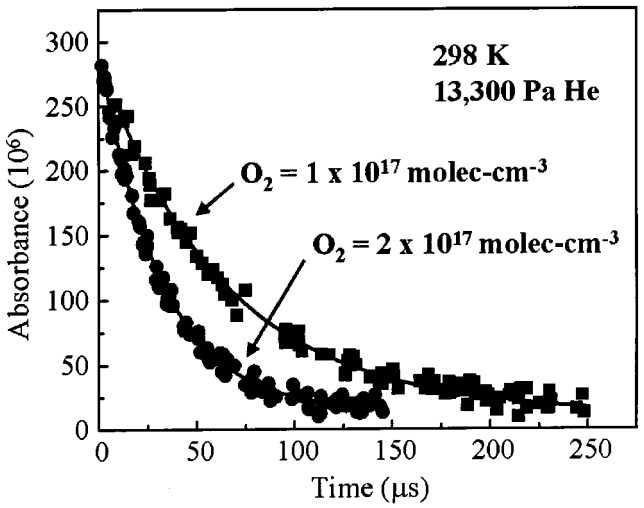

Figure 3. Two plots of the transient absorbance observed at 332.5 nm following the 193 nm photolysis of propargyl chloride at 295 K in the presence of added O_2. Each fit of the kinetic model (solid line) to the absorption signal yields an individual measurement of $k(C_3H_3+O_2)$. Increasing the O_2 density, which is in much higher concentration than the propargyl radical, leads to a linear increase in the observed rate coefficient. This relationship allows extraction of the bimolecular rate coefficient for each total pressure and third body. For both plots the total pressure is 13300 Pa (100 Torr) of He.

depletion of C_3H_3, thus, ruling out reaction of the propargyl radical with propargyl chloride.

Figure 2b shows typical experimental data observed for the photolysis of propargyl bromide. The line shows the fit computed by the kinetic model (Table 3) and lies in good agreement with the data. Unlike Cl atoms that react rapidly to depletion, Br atoms react slowly with propargyl bromide and persist for more than 1 ms after the photolysis event. The data support the assignment of a rapid cross-reaction between Br atoms and propargyl radicals (Table 3). The data indicates that propargyl radicals do not react with propargyl bromide. We also see no indication that reactions of HBr, a coproduct of C_3H_3Br photolysis, contribute to the observed decay, although this is less certain and would bear additional study. The cross reaction rate coefficient $k(C_3H_3+C_3H_3Br_2)$, derived from this 332.5 nm data (Table 3), is identical to the $k(C_3H_3+C_3H_3Br_2)$ obtained from a fit of 242 nm data.[30] The derived rate coefficient for the recombination of Br atoms with propargyl radicals (Table 3) seems to be of the right magnitude and to our knowledge represents its first determination.

Table 4 presents the kinetic mechanism used to fit absorption by C_3H_3 radicals following 193 nm photolysis of allene. Following the photolytic event, the absorption signal decays very rapidly and then slows (Figure 2c). The initial rapid decay arises from the reaction of photolytically produced H atoms with the propargyl radicals. After the H concentration is depleted by reactions with propargyl and allene molecules, slower reactions involving the propargyl and allyl radicals dominate the signal evolution.

The kinetic model includes side reactions involving allyl radicals. Allyl radicals should be the dominant reaction product of H+allene. When reacting with allene, an H atom may add to an end-carbon and form the vinyl radical, propene-2-yl, or an H atom may add to the center carbon and form the allyl radical. Because the allyl radical is resonance stabilized by 51 kJ mol^{-1} relative to the propene-2-yl radical,[37] the relative reverse reaction rates to H-atom loss will greatly favor the collisional stabilization of allyl radicals. For these fits we have fixed the cross-reaction rate coefficient to $k(C_3H_3+C_3H_5) = 2.9 \times 10^{-11}$ cm^3 molecule^{-1} s^{-1}, which is the mean of k_1 and $k(C_3H_5+C_3H_5)$.[38,39] Figure 2c shows the quality of a typical fit of the allene photolysis data which extracts individual measurements of $k(C_3H_3+H)$ and $k(C_3H_3+C_3H_3)$. Fits of signal traces of 100 μs to 3000 μs duration (100 points per trace) were used to derive the average rate coefficients reported in Table 4. Our derived rate coefficient for the reaction of H-atoms with propargyl radicals, $k(C_3H_3+H) = (2.5 \pm 1.1) \times 10^{-10}$ cm^3 molecule^{-1} s^{-1} is somewhat greater than the previously reported rate coefficient $k = 7.2 \times 10^{-11}$ cm^3 molecule^{-1} s^{-1}.[40] Nonetheless, our deduced rate coefficient is congruous with those obtained for similar hydrocarbon radicals (e.g., $k(H+C_2H_3) = 2.0 \times 10^{-10}$ cm^3 molecule^{-1} s^{-1} [41] and $k(H + \text{allyl}) = 3.3 \times 10^{-10}$ cm^3 molecule^{-1} s^{-1} [8]). Conceivably, differences in reaction conditions between the studies may explain this discrepancy. These previous studies were conducted in 266 Pa (≈2 Torr) helium.

To fit the C_3H_3 decay data, we did not need to assign a reactive role for C_3H_2, which is reported to comprise between 6%[24] and 21%[20] of the nascent reactive species produced by the photolysis event (reaction 3). The C_3H_2 carbene should react rapidly to depletion with allene, rendering its importance to the C_3H_3 decay as negligible except at the shortest times. Other possible side reactions including pseudo-first-order reactions of C_3H_3 radicals with the allene parent were considered and rejected by the model.

TABLE 5: Conditions Used to Determine the Rate Coefficient for Reaction 2, $k(C_3H_3+O_2)$, at 295 K

total pressure (Pa)/buffer gas	maximal O_2 density (10^{16} molecular cm^{-3})/ photolysis precursor	k_2 (10^{-13} cm^3 molecule^{-1} s^{-1})
1346/He	4.07/C_3H_3Cl	0.499
2671/He	5.15/C_3H_3Br	1.01
6657/He	13.4/C_3H_3Br	1.31
6663/He	15.6/C_3H_3Cl	1.29
9982/He	19.6/C_3H_3Cl	1.40
13327/He	26.4/C_3H_3Cl	1.35
1338/Ar	5.31/C_3H_3Br	0.985
303/N_2	6.45/C_3H_3Br	0.558
1330/N_2	4.31/C_3H_3Br	1.11
3402/N_2	14.6/C_3H_3Br	1.28
3353/N_2	12.4/C_3H_3Cl	1.40
6682/N_2	17.6/C_3H_3Cl	1.51
9995/N_2	26.3/C_3H_3Cl	1.77
13353/N_2	17.6/C_3H_3Cl	1.95

Oxygen Addition to Propargyl Radical. The termolecular association of molecular oxygen with the propargyl radical (reaction 2) was studied at 295 K in pseudo-first order with excess O_2. For each total pressure, 5 to 10 separate determinations of the observed first-order rate coefficient were conducted with varying O_2 densities. Figure 3 shows two typical plots from these determinations. The observed decays were fit to a combined second and first-order decay, using the second-order decay rate observed when there is no oxygen present. This treatment is much simpler than that used for the determination of the self-reaction rate coefficient and is justified by the much larger decay rate induced by the large excess of O_2. In fact, nearly identical rate coefficients are obtained by treating the system as purely pseudo-first order, but the mixed first and second order fitting procedure should be slightly more accurate. Table 5 presents the results of this investigation for three different buffer gases (third bodies) at total pressures ranging from 303 to 13300 Pa (2.28 to 100 Torr).

Figure 4 displays the results and also plots previous determinations of k_2. As observed previously by Slagle et al.,[9] the

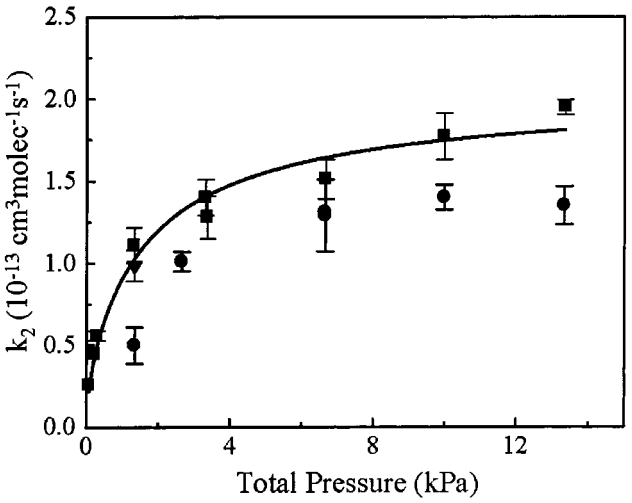

Figure 4. The bimolecular reaction rate coefficients derived for the termolecular association of propargyl radical with oxygen (reaction 2) as a function of total pressure of three different buffer gases (squares = N_2, circles = He, triangle = Ar). The solid line represents the fit of the N_2 buffer data using the conventional falloff expression ($F_c = 0.6$).[35] This fit yields the value, $k_2 = 2.3 \times 10^{-13}$ cm^3 molecule^{-1} s^{-1}. The two lowest pressure points represent the reported rate coefficients from Slagle, et al.[9]

reaction is in the falloff region between pure termolecular and saturated (bimolecular) behavior. A fit of the observed pressure dependence for the N_2 buffer to the falloff relationship[35] using a line-broadening factor ($F_c = 0.6$) yields the high-pressure limiting rate coefficient, $k_\infty = (2.3 \pm 0.2) \times 10^{-13}$ cm^3 molecule^{-1} s^{-1}, where the uncertainty is two standard deviations. As expected, the corresponding fit of data observed in He buffer yields the statistically indistinguishable rate coefficient, $k_\infty = 2.0 \pm 0.5 \times 10^{-13}$ cm^3 molecule^{-1} s^{-1}. Because the data sets for He and N_2 displayed little evidence of the linear (low) pressure regime, we did not attempt to model the combined data from both buffer systems using the three (or four) parameter fit described in the literature, although this procedure would likely have produced similar results.[42] Rather, because the N_2 data set is more complete and displays a greater degree of pressure saturation (as expected, N_2 is a better collisional stabilizer than He), we recommend the value derived from it, $k_\infty = (2.3 \pm 0.5) \times 10^{-13}$ cm^3 molecule^{-1} s^{-1}, where the stated uncertainty reflects the divergent results from the two buffer systems.

Discussion

Spectra and Photolysis End-Products. Previous studies have shown that, after exposure to 193 nm light, propargyl radicals are among the nascent photodissociation products of allene, propargyl chloride, and propargyl bromide. The present spectrum (Figure 1) and end-product analysis of the propyne photolysis products confirm that the 193 nm photolysis of propyne also leads to propargyl radicals. These results also agree with previous spectroscopic data.[11,12]

In accord with this study, Galli et al.[43] did not detect 2,4-hexadiyne among the mass analyzed stable products of propyne exposed to 206 nm light. The presence of 1,5-hexadiyne indicated that propargyl radicals dominated the recombination channels of the photoproducts. Thus, these observations of propargyl radical spectra and end-products comprise compelling evidence that propargyl radicals exist among the photolysis products of propyne.

In stark contrast to the results observed in higher pressure experiments, ample evidence, obtained under collisionless conditions, shows that the 1-propynyl radical is the nascent C_3H_3 species generated by photolysis of propyne with 193 nm light.[20,31,32] This evidence indicates that nascent $CH_3C{\equiv}C\bullet$, produced by reaction 5, is rapidly converted into a propargyl radical on a time scale that is short with respect to its self-reaction. Since the propargyl radical is 150 kJ mol^{-1} more stable than the $CH_3C{\equiv}C\bullet$ radical,[44] isomerization from the nascent 1-propynyl radical to the propargyl radical structures would reconcile the experimental data. However, the maximum available internal energy within the $CH_3C{\equiv}C\bullet$ photoproduct, 75 kJ mol^{-1}, is not sufficient to overcome the isomerization barrier of 144 kJ mol^{-1},[45] so isomerization does not occur rapidly.

Since the spectroscopic and end-product data were observed in experiments conducted in higher pressure systems, a secondary reaction may explain the appearance of propargyl radicals. In this view a nascent 1-propynyl radical, produced by reaction 5, reacts with a propyne molecule forming a propargyl radical and a propyne molecule:

$$CH_3C{\equiv}C\bullet + CH_3C{\equiv}CH \rightarrow CH_3C{\equiv}CH + \bullet CH_2C{\equiv}CH \quad (11)$$

Reaction 11 is approximately 36 kJ mol^{-1} exothermic.[46−48] The reactivity of the 1-propynyl radical should be similar to the analogous ethynyl radical, $HC{\equiv}C\bullet$, which rapidly abstracts a methyl hydrogen with rate coefficients ranging between $k = (1 \text{ to } 3.5) \times 10^{-11}$ cm^3 molecule^{-1} s^{-1}.[7,49,50] In the presence of a large partial pressure of propyne, as used in these present experiments, reaction 11 is likely to convert the nascent 1-propynyl radical population into propargyl radicals before reaction 8 can produce a detectable concentration of 2,4-hexadiyne. Additional experiments are needed to confirm this hypothesis.

Previous studies[6,9,11] have tersely noted soot deposits within their apparatus. Our observation that the deposition occurs exclusively in the photolysis region may be evidence that the subsequent reactions to form the PAHs (and thus the soot observed) may occur much more rapidly at the surface of the uncoated reactor than in the gas phase. This would not be a surprising result, but it could be important in the interpretation of kinetic data where the mixture is in intimate contact with the walls of a reactor. In the laser photolysis/CRD reactor, the probed volume is much smaller than the total reaction volume and is displaced away from the walls. The time required for wall reaction products to diffuse back into the observation zone is expected to be comparable to the observation times in the current study, resulting in minimal perturbation from wall reactions, particularly for the higher pressures.

Reaction Rate Coefficients. During this study the self-reaction rate coefficients derived from simple second-order fits to time dependent absorption (and hence concentration) data were observed to vary with the photolysis precursor choice. This observation was taken as evidence of the presence of side reactions, which also contribute to the loss of the observed propargyl radical absorption. Thus, we subjected the data to more complex analyses, using a numerical forward integration of a reaction mechanism and subsequent variation of the rate parameters to obtain a fit. Our mechanisms account for all of the radical (atomic) products of the photolysis and subsequent reactions. Chief among these for all of the precursor molecules was reaction of a halogen or hydrogen atom with the parent to form a new highly reactive radical, which then participated in the destruction of the propargyl radical. The observation of some of these new radicals in absorption near 240 nm and their kinetic behavior greatly aided in the development of this mechanism.

All three kinetic models fit the data with nearly the same propargyl self-reaction rate coefficient. This accord in k_1 was reached by accounting for the side reactions of C_3H_3 with the companion radicals that were cogenerated by the photolysis event of each precursor. The weighted average of the three k' rate coefficients is $k_1 = (4.3 \pm 0.6) \times 10^{-11}$ cm^3 molecule^{-1} s^{-1}, where the uncertainty denotes two standard deviations and includes the propagated uncertainty of the absorption coefficient, $\sigma_{332.5}$. Although the kinetic complexity of these reactive systems caused us to discard simple analyses based on second-order fits of the C_3H_3 decays, such rate coefficients give a rough assessment of the total reactivity observed within an experiment. Second-order fits of C_3H_3 decay data obtained by photolyzing propargyl chloride and propargyl bromide gave k_1'(second order) $= (8.3 \pm 1.7) \times 10^{-11}$ cm^3 molecule^{-1} s^{-1} and k_1'(second order) $= (6.6 \pm 0.8) \times 10^{-11}$ cm^3 molecule^{-1} s^{-1}, respectively. The similar magnitude of these rate coefficients is consistent with our assignment that the cross reactants with C_3H_3 are members of the same chemical class. These cross reactants are dihalogenated vinyl radicals,[30] where $C_3H_3Cl_2$ is more reactive toward C_3H_3 than is $C_3H_3Br_2$.

The present rate coefficient k_1 is significantly smaller than those reported by Morter et al.[6] who used the same halogenated precursors and photolysis wavelength. Some discord is expected because they fit their C_3H_3 decays to a second-order rate coefficient. Thus, their analysis did not consider the side reactions that destroy propargyl radicals. We note that their tests for interference from photolytic Cl atoms may have proved inadequate to detect (or suppress) the chlorine addition to propargyl chloride (reaction 4) that occurs at nearly the collision rate (Table 2). However, these differences in the treatment of side reactions only account for a lesser portion of the observed discrepancy.

The previously reported rate coefficient is nearly twice what we derive from a simple second-order fit to the data in the C_3H_3-Cl system (to which it should be comparable). Moreover, Morter et al.[6] reported that the k_1(second order) derived by fitting their C_3H_3Br photolysis data was a factor of 2 larger than the k_1-(second order) derived from their C_3H_3Cl photolysis data. Those relative rates indicate that the photolysis of propargyl bromide created a much more reactive chemical environment within their apparatus than was created during the photolysis of propargyl chloride. The authors postulated that the origin of this variance was a greater photolytic production of C_3H_2 + HBr and the subsequent reaction of one or both of these species with propargyl radicals. In the present study we see no indication that this is the case. Indeed, simple second-order fits to our decay signatures following the photolysis of C_3H_3Br indicate that it is a less reactive system toward propargyl radicals. We note that Morter et al.[6] used propargyl bromide drawn from a toluene solution. The introduction of trace amounts of toluene into their reaction mixture may have introduced additional depletion channels for propargyl radicals through reactions with toluene and its molecular and atomic (e.g., H atom) photofragments. We also note that the IR absorption experiments observed gas samples that were exposed to several photolysis pulses. The accumulation of secondary photoproducts may have spawned additional propargyl radical sinks, accelerating the apparent k_1-(second order) for both photolysis systems during their study.

The rate coefficients for the association reaction of propargyl with oxygen (reaction 2) obtained in this study concur with those measured using the sampled flow/mass spectrometer system.[9] As reported earlier, at 295 K reaction 2 proceeds by essentially irreversible addition and resides in the falloff region between linear and saturated pressure dependence. The high-pressure limiting-rate coefficient $k_\infty = (2.3 \pm 0.5) \times 10^{-13}$ cm^3 molecule^{-1} s^{-1} derived by this study (Figure 4) is lower than the oxygen addition rate coefficients for saturated hydrocarbon radicals (e.g., ethyl + O_2, *n*-propyl + O_2, $k_\infty = 8.0 \times 10^{-12}$ cm^3 molecule^{-1} s^{-1} [35,51]). This k_∞ is also lower than those of unsaturated radicals which do not possess resonance stabilization (e.g., vinyl +O_2, $k_\infty = 1.0 \times 10^{-11}$ cm^3 molecule^{-1} s^{-1}).[52]

Conclusion

The self-reaction and oxygen termolecular association rate coefficients for the propargyl radical have been measured at 295 K and pressures ranging from 300 to 13300 Pa (2.25 to 100 Torr) of three different buffer gases using the laser photolysis/cavity ring-down technique. The self-reaction, which is an important route to polycyclic aromatic hydrocarbons in sooting flames, was found to be pressure independent across the entire pressure range for all of the buffers. The data analyses used chemical models that accounted for side reactions that were undetected in previous studies. These models were used to fit absorption data of C_3H_3 observed during from the photolysis of allene, propargyl chloride, and propargyl bromide. The fit of all three reaction systems obtains the current recommendation, $k_1 = (4.3 \pm 0.6) \times 10^{-11}$ cm^3 molecule^{-1} s^{-1}. This rate coefficient is only about 20% smaller than that determined in the temperature range 623−673 K, $k_1 = 5.7 \times 10^{-11}$ cm^3 molecule^{-1} s^{-1}, implying that the high pressure limiting-rate coefficient for this reaction has essentially no temperature dependence as is often seen for radical−radical recombination reactions. The association reaction with molecular oxygen (reaction 2) was found to be in the falloff region between linear and saturated pressure dependence for the three buffer gases used here (Ar, He, and N_2) in the pressure range between 300 and 13300 Pa. The high-pressure limiting-rate coefficient $k_\infty = 2.3 \times 10^{-13}$ cm^3 molecule^{-1} s^{-1} was derived using the standard falloff relationship[35] and is much lower than the coefficients of comparable hydrocarbon radicals with O_2. This is the expected result for the resonance stabilized propargyl radical and is important in determining the sooting effect of propargyl radicals in flames.

Acknowledgment. We thank Drs. Askar Fahr, Jeffrey A. Manion, and Wing Tsang for insightful discussions and assistance with some experiments.

References and Notes

(1) Tsang, W. *Int. J. Chem. Kinet.* **1978**, *10*, 687.
(2) King, K. D. *Int. J. Chem. Kinet.* **1978**, *10*, 545.
(3) Miller, J. A.; Melius, C. F. *Combust. Flame* **1992**, *91*, 21.
(4) Alkemade, U.; Homann, K. H. *Z. Phys. Chem. (Neue Folge)* **1989**, *161*, 19.
(5) Wu, C. H.; Kern, R. D. *J. Phys. Chem.* **1987**, *91*, 6291.
(6) Morter, C. L.; Farhat, S. K.; Adamson, J. D.; Glass, G. P.; Curl, R. F. *J. Phys. Chem.* **1994**, *98*, 7029.
(7) Tsang, W. *J. Phys. Chem. Ref. Data* **1988**, *17*, 887.
(8) Tsang, W. *J. Phys. Chem. Ref. Data* **1991**, *20*, 221.
(9) Slagle, I. R.; Gutman, D. *Symp. Int. Combust. Proc.* **1988**, *21*, 875.
(10) Atkinson, D. B.; Hudgens, J. W. *J. Phys. Chem. A* **1997**, *101*, 3901.
(11) Ramsay, D. A.; Thistlethwaite, P. *Can. J. Phys.* **1966**, *44*, 1381.
(12) Jacox, M. E.; Milligan, D. E. *Chem. Phys.* **1974**, *4*, 45.
(13) Certain commercial materials and equipment are identified in this paper in order to adequately specify the experimental procedure. Such identification neither implies recommendation or endorsement by the National Institute of Standards and Technology nor does it imply that the material or equipment identified is the best available for the purpose.
(14) Nonlinear Levenberg−Marquardt fitting virtual instrument. Labview 4.0; National Instruments Corporation: Austin, TX, 1994−1995.
(15) Braun, W. *Int. J. Chem. Kinet.* **1988**, *20*, 51.

(16) Honjou, H.; Yoshimine, M.; Pacansky, J. *J. Phys. Chem.* **1987**, *91*, 4455.
(17) Botschwina, P.; Oswald, R.; Flügge, J.; Horn, M. *Z. Phys. Chem.* **1995**, *188*, 29.
(18) Fahr, A.; Hassanzadeh, P.; Laszlo, B.; Huie, R. E. *Chem. Phys.* **1997**, *215*, 59.
(19) Jackson, W. M.; Anex, D. S.; Continetti, R. E.; Balko, B. A.; Lee, Y. T. *J. Chem. Phys.* **1991**, *95*, 7327.
(20) Sun, W.; Yokoyama, K.; Robinson, J. C.; Suits, A. G.; Neumark, D. M. *J. Phys. Chem.* **1999**, *110*, 4363.
(21) Slagle, I. R.; Gmurczyk, G. W.; Batt, L.; Gutman, D. *Symp. Int. Combust. Proc.* **1990**, *23*, 115.
(22) Jackson, W. M.; Mebel, A. M.; Lin, S. H.; Lee, Y. T. *J. Phys. Chem. A* **1997**, *101*, 6638.
(23) Mebel, A. M.; Jackson, W. M.; Chang, A. H. H.; Lin, S. H. *J. Am. Chem. Soc.* **1998**, *120*, 5751.
(24) Song, X.; Bao, Y.; Urdall, R. S.; Gosine, J. N.; Jackson, W. M. *Chem. Phys. Lett.* **1994**, *217*, 216.
(25) Seburg, R. A.; Paterson, E. V.; Stanton, J. F.; McMahon, R. J. *J. Am. Chem. Soc.* **1997**, *119*, 5847.
(26) Stanton, J. F.; DePinto, J. T.; Seburg, R. A.; Hodges, J. A.; McMahon, R. J. *J. Am. Chem. Soc.* **1997**, *119*, 429.
(27) Merer, A. J. *Can. J. Phys.* **1967**, *45*, 4103.
(28) Jacox, M. E. *J. Phys. Chem. Ref. Data* **1998**, *27*, 115.
(29) Jacox, M. E. *J. Phys. Chem. Ref. Data* **1994**, *13*, 461.
(30) Atkinson, D. B.; Hudgens, J. W. Chlorination chemistry I: Rate Coefficients, reaction mechanisms, and spectra of the chlorine and bromine adducts of propargyl halides. In press.
(31) Seki, K.; Okabe, H. *J. Phys. Chem.* **1992**, *96*, 3345.
(32) Satyapal, S.; Bersohn, R. *J. Phys. Chem.* **1991**, *95*, 8004.
(33) Samples of propargyl chloride and propyne illuminated with 193 nm laser light and injected into the gas chromatograph were observed to elute a strong peak 6 min after sample injection. This eluted peak produced a mass spectrum that matched precisely with 1,5-hexadiyne. The weaker, unidentified C_6H_6 species eluted from the column at 7.2 min and produced a mass spectrum with relative abundances of *m*/*z* 78 (100), *m*/*z* 77 (60), *m*/*z* 52 (38), *m*/*z* 51 (52), *m*/*z* 50 (43), *m*/*z* 40 (78), *m*/*z* 39 (46), *m*/*z* 38 (14). The relative abundance of *m*/*z* 40 is unreliable due to a small amount of Ar contamination from leaked air. We further note that the ratio of *m*/*z* 77, 78 does not support an assignment of the eluent to 2,4-hexadiyne and that the triplet at *m*/*z* 52−50 is very distinct. The overall spectrum of this species does not resemble the mass spectra of both known diynes.
(34) Hodges, J. T.; Looney, J. P.; van Zee, R. D. *Appl. Optics* **1996**, *35*, 4112.
(35) DeMore, W. B.; Sander, S. P.; Golden, D. M.; Hampson, R. F.; Kurylo, M. J.; Howard, C. J.; Ravishankara, A. R.; Kolb, C. E.; Molina, M. J. Chemical kinetics and photochemical data for use in stratospheric modeling. National Aeronautics and Space Administration: Washington, DC, 1994.
(36) Halberstadt, M. L.; Crump, J. *J. Photochem.* **1973**, *1*, 295.
(37) Tsang, W.; Walker, J. A. *J. Phys. Chem.* **1992**, *96*, 8378.
(38) Tulloch, J. M.; Macpherson, M. T.; Morgan, C. A.; Pilling, M. J. *J. Phys. Chem.* **1982**, *86*, 3812.
(39) Jenkin, M. E.; Murrells, T. P.; Shalliker, S. J.; Hayman, G. D. *J. Chem. Soc., Faraday Trans.* **1993**, *89*, 433.
(40) Homann, K. H.; Wellmann, C. *Ber. Bunsen-Ges. Phys. Chem.* **1983**, *87*, 609.
(41) Fahr, A.; Laufer, A.; Klein, R.; Braun, W. *J. Phys. Chem.* **1991**, *95*, 3218.
(42) Kurylo, M. J.; Ouellette, P. A. *J. Phys. Chem.* **1986**, *90*, 441.
(43) Galli, A.; Harteck, P.; Reeves, R. R., Jr. *J. Phys. Chem.* **1967**, *71*, 2719.
(44) Collin, G. J.; Deslauriers, H.; DeMare, G. R.; Poirier, R. A. *J. Phys. Chem.* **1990**, *94*, 134.
(45) Vereecken, L.; Pierloot, K.; Perters, J. *J. Chem. Phys.* **1998**, *108*, 1068.
(46) Robinson, M. S.; Polak, M. L.; Bierbaum, V. M.; DePuy, C. H.; Lineberger, W. C. *J. Am. Chem. Soc.* **1995**, *117*, 6766.
(47) Wagman, D. D.; Kilpatrick, J. E.; Pitzer, K. S.; Rossini, F. D. *J. Res. NBS* **1945**, *35*, 467.
(48) Chase, M. W., Jr.; Davies, C. A.; Downey, J. R., Jr.; Frurip, D. J.; McDonald, R. A.; Syverud, A. N. *J. Phys. Chem. Ref. Data* **1985**, 14.
(49) Tsang, W. *J. Phys. Chem. Ref. Data* **1987**, *16*, 471.
(50) Opansky, B. J.; Leone, S. R. *J. Phys. Chem.* **1996**, *100*, 19904.
(51) Atkinson, R.; Baulch, D. L.; Cox, R. A.; Hampson, R. F., Jr.; Kerr, J. A.; Troe, J. *J. Phys. Chem. Ref. Data* **1992**, *21*, 1125.
(52) Knyazev, V. D.; Slagle, I. R. *J. Phys. Chem.* **1995**, *99*, 2247.
(53) Warnatz, J. Rate coefficients in the C/H/O system. In *Combustion Chemistry*; Gardiner, W. C., Ed.; Springer-Verlag: New York, 1984; p 197.
(54) Tsang, W.; Hampson, R. F. *J. Phys. Chem. Ref. Data* **1986**, *15*, 1087.